

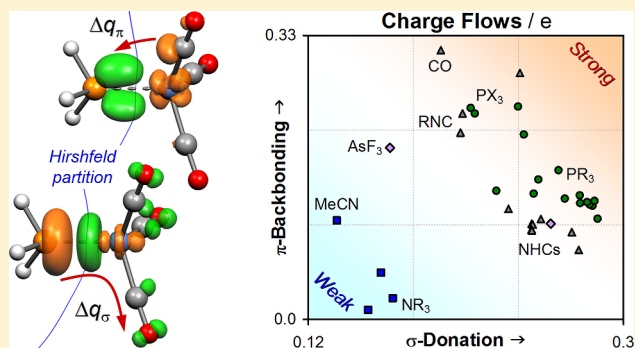
Intuitive Quantifiers of Charge Flows in Coordinate Bonding

Erik P. A. Couzijn,^{†,‡} Yu-Ying Lai,^{†,§} Armin Limacher, and Peter Chen^{*:ib}

Laboratorium für Organische Chemie, ETH Zürich, Vladimir-Prelog-Weg 2, CH-8093 Zürich, Switzerland

Supporting Information

ABSTRACT: ETS–NOCV charge and bond energy analyses have been carried out for a broad range of transition-metal carbonyl complexes $L-[M]$, comprising different ligand classes, transition metals, and coordination geometries. The resulting electronic redistributions are visually assigned to σ donation, π backbonding, and related interactions. We propose a Hirshfeld partitioning of these electronic redistributions to afford the corresponding charge flow contributions Δq_σ , Δq_π etc. Taken together, a detailed picture of the dative bonding arises, in terms of both energetics and the extent of σ -electron donation and π -electron backbonding. The charge flows Δq_σ and Δq_π appropriately quantify trends in the ligand σ -donor and π -acceptor abilities and are transferable across the transition-metal complexes studied and thus promise to be suitable descriptors for ligand knowledge bases. As a case in point, the TEP is well reproduced by the calculated $\nu_{CO}(A_1)$ frequencies and is 3 times more strongly affected by Δq_σ than by Δq_π with an additional modest steric influence. Further, empirical relationships are derived among the charge flows Δq_σ and Δq_π , the $(L)W(CO)_5$ carbonyl stretching frequencies, and the ligand's steric volume $\%V_{bur}$, which allow estimating the σ -donor and π -acceptor abilities of phosphines from experimental observables. On the other hand, direct $Cl \rightarrow L-\sigma^*$ interactions are identified in several *cis*-(L) $Ir(CO)_2Cl$ complexes, which compromises the use of these species as experimental probes for ligand parameters.



INTRODUCTION

The chemical and physical properties of transition-metal complexes are primarily determined by the electronic and steric influence of the ligands. Several models have been developed to describe these ligand properties,¹ of which the Tolman Electronic Parameter (TEP) is well-established and is widely used to guide the fine-tuning of organometallic complexes, e.g. in homogeneous catalysis. The TEP corresponds to the CO A_1 stretching frequency of complexes $(L)Ni(CO)_3$, as originally determined for various P-donor ligands;² a lower $\nu_{CO}(A_1)$ value indicates a more strongly electron donating ligand on account of increased metal to carbonyl π backbonding. The TEP was later used to quantify the electronic properties of other ligands, including N-heterocyclic carbenes (NHCs) and divalent carbon(0) compounds.³ Different metal complexes, such as square-planar *cis*-(L) $M(CO)_2Cl$ ($M = Ir, Rh$) that are easier to prepare and handle, have been studied and their CO stretching frequencies were correlated to the TEP.⁴

Tolman ascribed the coordinating power of ligands primarily to their σ -donor and π -acceptor abilities,² but the TEP is a measure only of their *net* donor strength. Moreover, recent studies question its reliability for multiple reasons.⁵ The TEP performs poorly when different ligand types are compared^{5a} and fails to describe the bonding trends in linear gold complexes, which are governed by π backbonding.^{5b} In addition, the CO stretching frequencies were shown to be affected by through-space ligand interactions^{5c} and by mode

coupling between vibrations.^{5d,e} Thus, there is a need for alternative descriptors to build ligand knowledge bases with more predictive power.

Several models have been proposed to unravel the TEP and to offer more suitable ligand electronic parameters.^{5b–e,6} However, the sophisticated method QALE (quantitative analysis of ligand effects)^{6a–c} relies intricately on a variety of experimental data, which prohibits its use in predicting the coordination properties of novel ligands under design. The theoretical parameters CEP (computationally derived ligand electronic parameter, i.e. calculated $\nu_{CO}(A_1)$ for $(L)Ni(CO)_3$),^{6d} LTEP (local TEP, i.e. mode-decoupled $\nu_{CO}(A_1)$),^{5d} MESP (molecular electrostatic potential minimum at the ligand's lone pair region),^{6e–g} and the average local ionization energy^{6h} do not have this limitation, but in turn they do not provide a straightforward separation into σ -donor and π -acceptor contributions. The same is true for the metal–ligand electronic parameter (MLEP, i.e. local $L-Ni(CO)_3$ bond force constant), which could be derived from experimental data but so far has been computed.^{5e}

In a different vein, the ligand–metal bonding has been described in detail either on the basis of the total electron density or energetically by various quantum chemical methods.^{7–14} In the first category fall the quantum theory of atoms in molecules (QTAIM),⁸ which computes properties

Received: May 11, 2017

Published: August 28, 2017

over atomic basins and bond paths derived from the topology of the total density; the natural bond orbital (NBO)⁹ description as an optimal Lewis structure with second-order perturbations; and the charge decomposition analysis (CDA)¹⁰ in terms of the fractions of electrons shared between orbitals of both fragments. On the other hand, the bonding energetics can be dissected by the constrained space orbital variation (CSOV)¹¹ method of sequentially relaxing and mixing each of the superposed fragment wave functions or by the extended transition state (ETS)¹² model in terms of fragment preparation, electrostatic interaction, Pauli repulsion, and orbital interactions partitioned by symmetry. The recent natural orbitals for chemical valence (NOCV) model¹³ extends ETS by extracting the principal electronic redistributions occurring upon bonding, which usually can be readily assigned to e.g. σ and π interactions,^{13g} and the orbital interactions are partitioned accordingly. While the aforementioned analyses deliver a wealth of detailed insights, their execution and interpretation requires considerable expertise and some methods are impracticable for larger, nonsymmetric complexes. Furthermore, the obtained ligand bonding parameters are often not readily transferable to other series of complexes (see also below).

In this article, we introduce intuitive computational parameters that quantify and dissect the amount of charge transfer for each bonding mode in transition-metal complexes. The chemical bonding of a wide range of ligands in various metal–carbonyl complexes is investigated with the ETS–NOCV charge and energy decomposition scheme.^{12,13} We apply the Hirshfeld partitioning¹⁵ to the resulting NOCV electronic redistributions—which are matched to σ , π , and related bonding contributions by visualization^{13g}—to obtain associated charge flows. These charge flow contributions quantify how many electrons move from the ligand to the metal fragment or vice versa through each binding mode, which is a straightforward definition of the σ -donating and π -accepting ability of a ligand in a transition-metal complex. We show that the charge flow contributions reproduce commonly accepted trends in ligand electronic properties and are well correlated across complexes of different transition metals and coordination geometries. A couple of anomalies are attributed to additional specific interactions that are also apparent from the NOCV electronic redistributions and from structural features. Next, we relate the L–Ni(CO)₃ charge flows to $\nu_{\text{CO}}(A_1)$ frequencies in order to dissect the TEP into σ -donor, π -acceptor, and steric influences. Finally, empirical equations are derived for estimating the charge flow contributions from spectroscopic data for P-donor W(CO)₅ complexes. Thus, the proposed method builds a bridge between theoretical and experimental concepts in transition-metal chemistry, highlights some of the complications in constructing accurate empirical models using ligand knowledge bases, and offers predictive power in ligand design.

EXPERIMENTAL SECTION

All experiments were carried out under an argon or CO atmosphere using standard Schlenk techniques and dried and degassed solvents. Selected tetracarbonyliron(0) complexes were synthesized to confirm their carbonyl stretching frequencies in apolar solvent. FT-IR spectra were recorded on a PerkinElmer Spectrum Two instrument equipped with ATR (trimethylamine complex) or a PerkinElmer Paragon 1000 apparatus. As most of the substances slowly decompose in solution, a small amount of sample was dissolved in the specified alkane immediately prior to analysis. The CO₂ absorption band at 667

cm⁻¹ was included in the spectrum and used as internal reference. Further details, including NMR characterizations, are contained in the Supporting Information.

Tetracarbonyl(pyridine)iron(0) was synthesized following a literature procedure.^{16a} FT-IR (*n*-hexane + pyridine): 2051.0, 1966.8, 1941.3, 1907.4 cm⁻¹.

Tetracarbonyl(trimethylamine)iron(0) was synthesized following a literature procedure.^{16b} FT-IR (*n*-heptane): 2049.9, 1963.7, 1932.9 cm⁻¹.

Tetracarbonyl(tris(*tert*-butyl)phosphine)iron(0) was synthesized following a literature procedure.^{16c} FT-IR (*n*-hexane): 2042.3, 1964.7, 1926.2, 1892.0 cm⁻¹.

Tetracarbonyl(triphenylphosphine)iron(0) was synthesized analogously to the tris(*tert*-butyl)phosphine complex. In a Schlenk tube under an inert atmosphere, triiron(0) dodecacarbonyl (0.52 g, 1.0 mmol) was dissolved in dry methanol (25 mL) and triphenylphosphine (780 mg, 2.97 mmol) was added. The mixture was sonicated at 50 °C for several hours. All volatiles were removed under vacuum, and the residue was redissolved in *n*-hexane and extracted with acetonitrile. The product was recrystallized from the hexane phase. FT-IR (*n*-hexane): 2050.0, 1977.4, 1944.3, 1909.1 cm⁻¹.

Computational Methods. Density functional theory (DFT) calculations were performed with ADF 2010¹⁷ at the BP86/ZORA/TZP level of theory;¹⁸ see section 2 in the Supporting Information for details. All structures were optimized and subjected to frequency analyses to confirm that they are minima and to obtain the CO stretching frequencies ν_{CO} . The ligand steric parameter % V_{bur} was determined from the optimized *cis*-(L)Ir(CO)₂Cl structures analogously to the procedure of Cavallo and Nolan (see section 2.2 in the Supporting Information),¹⁹ taking a coordination sphere of 3.50 Å radius at 2.10 Å from the donor atom; % $V_{\text{bur}}(\text{Ni})$ was determined accordingly with a 3.50 Å sphere at Ni in the optimized (L)Ni(CO)₃ complexes.

The ETS–NOCV scheme (also named EDA–NOCV after the energy decomposition analysis of ADF that implements the ETS model) was applied to study the interactions of 34 ligands L with metal fragments Ni(CO)₃, *cis*-Ir(CO)₂Cl, Fe(CO)₄, and W(CO)₅ as a ligand to metal dative bond is formed to afford complexes L–Ni(CO)₃, *cis*-L–Ir(CO)₂Cl, *ax*-L–Fe(CO)₄, and L–W(CO)₅. The extended transition state (ETS) method decomposes the net bonding energy BDE into four contributions:¹⁷ the preparation energy ΔE_{prep} required to bring the separate fragments from their optimum spatial and electronic structures to those in the total molecule, the electrostatic attraction (ΔV_{elstat}) and Pauli repulsion (ΔE_{Pauli}) between the fragments, and the total orbital interaction energy ΔE_{oi} reflecting the stabilization energy gained by relaxation of the sum-of-fragments electron density to that of the total molecule:

$$-\text{BDE} = \Delta E_{\text{prep}} + (\Delta V_{\text{elstat}} + \Delta E_{\text{Pauli}}) + \Delta E_{\text{oi}} \quad (1)$$

The difference between the sum-of-fragments density ρ_{sumfrag} and that of the total molecule ρ_{mol} is called the deformation density $\Delta\rho$. Mathematically, NOCV analysis¹³ represents $\Delta\rho$ as a sum of pairs of complementary eigenvectors (ψ_{-i} , ψ_i) with corresponding eigenvalues ($-\varepsilon_i$, ε_i) that are equal in magnitude but opposite in sign. Chemically speaking, the NOCV pairs (ψ_{-i} , ψ_i) are donor and acceptor orbitals and ε_i denotes the net electron transfer from donor to acceptor orbital. This brings about an electronic redistribution $\Delta\rho_i$ with associated contribution ΔE_i to the total orbital interaction energy, which can be computed according to eqs 2 and 3:

$$\Delta\rho(\vec{r}) = \sum \Delta\rho_i(\vec{r}) = \sum \varepsilon_i[-\psi_{-i}^2(\vec{r}) + \psi_i^2(\vec{r})] \quad (2)$$

$$\Delta E_{\text{oi}} = \sum \Delta E_i = \sum \varepsilon_i[-F_{-i,-i}^{\text{TS}} + F_{i,i}^{\text{TS}}] \quad (3)$$

where F^{TS} is the Kohn–Sham matrix defined over NOCVs with respect to the transition state density (being the average of ρ_{sumfrag} and ρ_{mol}).¹⁷ Typically only few NOCV pairs contribute significantly to the bonding, and visualization of each electronic redistribution $\Delta\rho_i$ usually allows unambiguous assignment as, e.g., σ - or π -type bonding.^{13g}

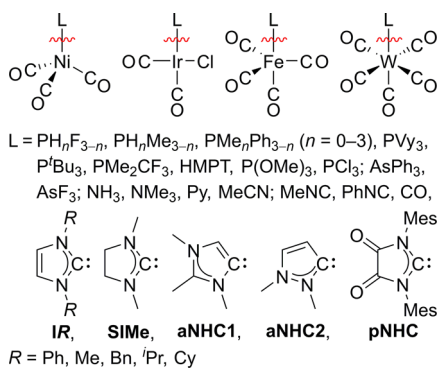
Exemplary electronic redistributions for the complexes studied in this article are depicted in section 2.6 in the Supporting Information.

Preliminary Hirshfeld partitionings¹⁵ of the electronic redistributions (see the main text) were performed with a standalone C program that numerically integrates density data from the TAPE21 file using a cubic grid. After this proof of concept, the partitioning was implemented by SCM in a development version of ADF (build 201302062204), providing superior integration accuracy and workflow efficiency. The charge flow analysis is now available in the ADF2017 release through the keyword “PRINT NOCVHirshfeld”.

RESULTS AND DISCUSSION

Scheme 1 lists the 34 ligands L and 4 metal carbonyl fragments [M] studied, encompassing different donor elements, transition

Scheme 1. Complexes Studied^a



^aAbbreviations: Vy = vinyl, HMPT = hexamethylphosphorane triamide, Mes = 2,4,6-trimethylphenyl.

metals, and coordination geometries. A comprehensive range of ligand types was considered, including phosphines, arsines, amines, pyridine, (iso)nitriles, CO, and NHCs. Several of these complexes have been experimentally synthesized and characterized.

Ligand Bonding Decompositions. The ligand–metal bonding in the complexes in Scheme 1 is usually described in analogy to the Dewar–Chatt–Duncanson (DCD) model for alkene π complexes.^{21,14d,13b,f} That is, both the ligand and the metal fragment have a singlet electronic ground structure and engage in synergistic σ donation, from the ligand’s lone electron pair into the metal’s d_z^2 orbital, and π backbonding, from the metal’s d_{xz} and/or d_{yz} orbitals into antibonding π^* ligand orbitals. The L–[M] net bond energies were decomposed accordingly within the ETS–NOCV framework. For most of the complexes, only the first four NOCV pairs were found to contribute significantly to the coordinative bonding. As reported previously^{13g} and as illustrated for $(\text{PH}_3)\text{Ni}(\text{CO})_3$ in Figure 1, the associated electronic redistributions $\Delta\rho_i$ are readily assigned to $L \rightarrow M$ σ -donation, $L \leftarrow M$ π backbonding (in two orthogonal planes along the L–M bond), and a modest σ back-donation from primarily the metal’s d_z^2 orbital into the lowest-energy A_1 -symmetric σ^* orbital of the ligand;^{13g} see the Supporting Information for all decomposition results and further examples.

The depicted electronic redistributions not only illuminate the primary bonding interactions (e.g., donation of part of the ligand’s lone electron pair into the bonding region, Figure 1 left) but also feature clear contributions on the carbonyl moieties. The $L \rightarrow M$ σ -donating interaction is accompanied by an accumulation of charge from the metal d_z^2 orbital into the

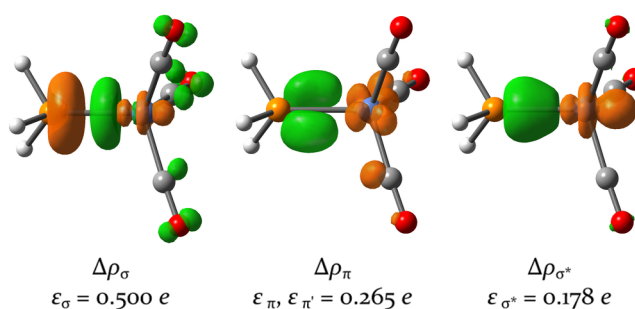


Figure 1. Main electronic redistributions for the $\text{H}_3\text{P-Ni}(\text{CO})_3$ bonding. Green and orange contours signify charge density accumulation and depletion, respectively (σ , ± 0.004 au; π , ± 0.002 au, one of two equivalent contributions shown; σ^* , ± 0.001 au); note that these contours do *not* represent orbitals with phases.

CO π systems, reflecting the increased $M \rightarrow \pi^*_{\text{CO}}$ backbonding that is responsible for the small TEP observed for strong σ -donor ligands. Conversely, the $L \leftarrow M$ π backbonding from the metal d_{xz} and d_{yz} orbitals features a depletion of charge in the CO π systems, reflecting the competition with $M \rightarrow \pi^*_{\text{CO}}$ backbonding that leads to a larger TEP.

ETS–NOCV Descriptors. We first tested whether the NOCV eigenvalues ε_σ and ε_π (as did Mitoraj et al.^{13g}) or the orbital interaction energies ΔE_σ and ΔE_π would be suitable to quantify the magnitude of the σ -donating and π -backbonding interactions, respectively. However, both ε_σ and ΔE_σ for $L\text{-Ni}(\text{CO})_3$ are found to correlate poorly with those for the other three series of complexes (see section 3.3 in the Supporting Information), and in part separate trends can be recognized for the different ligand classes. For ε_σ this is likely due to the fact that the related electronic redistribution $\Delta\rho_\sigma$ also contains contributions from polarizations *within* both the ligand and the metal fragment. ΔE_σ , on the other hand, depends intricately on the energy gaps and overlaps between the ligand’s lone pair—being a variable admixture of the coordinating element’s valence s and p_z orbitals—and the metal’s interacting s , p_z , and d_z^2 orbitals (Figure 2, left). This affords a set of molecular

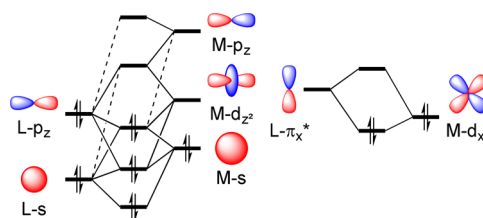


Figure 2. Basic orbital interaction diagrams for $L \rightarrow M$ σ donation (left; energy levels not drawn to scale) and $L \leftarrow M$ π backbonding (right; analogous interaction in the yz plane not shown).

orbitals (MOs) for which a change in the total σ -bonding stabilization energy is hard to trace back to individual perturbations in fragment orbital energy levels and overlaps, undermining any simple correlation. In addition, the extent and diffuseness of the L s vs L p_z orbital depends differently on the coordinating element and, as a result, their relative contributions will differ in the bonding of the various ligand classes.

We note that, for π backbonding, acceptable to good correlations across the series of complexes are found for $\sum \varepsilon_\pi$ and for $\sum \Delta E_\pi$ (summing the two mutually orthogonal $L \leftarrow M$ π -backbonding contributions). At least for the complexes

studied here, the basic L π^* –M d orbital interaction scheme (Figure 2, right) is less complicated than that for σ donation. The coordinating element plays only a minor role because along with the L π^* orbitals also the L s and L p_z orbitals become more extended/compact, leading to a longer/shorter L–M bond, which in part offsets the effects on the L $\pi_{x/y}^*$ –M $d_{xz/yz}$ overlaps. Hence, the ligand- and metal-dependent perturbations to the energy gaps and orbital overlaps appear to affect the π -bonding stabilization energy $\sum \Delta E_\pi$ in a quite straightforward, proportional way. However, this is not self-evident: perturbations that invert the ordering of the L π^* and M d energy levels would break the monotony of the trend. Further, like ε_σ , also $\sum \varepsilon_\pi$ includes intrafragment polarizations, which for other complexes may be manifested in a less orderly manner than is apparently the case here.

All in all, neither the NOCV eigenvalues ε_i nor the orbital interactions ΔE_i are suitable as general descriptors of the ligand electronic properties in coordinate bonding.

Charge Flow Contributions Δq_σ and Δq_π . As mentioned above, the electronic redistributions $\Delta\rho_i$ consist of polarizations between as well as within the fragments: i.e., they extend over the whole complex. We realized that the flow of charge from the ligand to the metal moiety or vice versa, as induced by an NOCV interaction i , could be quantified by partitioning the corresponding electronic redistribution $\Delta\rho_i$ between both fragments. This should provide a much better description of the dative bonding character than the eigenvalues ε_i discussed above, as the unrelated polarizations within each fragment are disregarded. A well-established procedure that suits our purpose is the Hirshfeld partitioning,¹⁵ in which the property of interest is integrated over space, at each point weighted by the ratio between the chosen fragment and the sum-of-fragments electron densities. Accordingly, each electronic redistribution $\Delta\rho_i$ affords a charge flow contribution Δq_i^{frag} as expressed by eq 4, with illustrations for $\Delta q_\sigma^{[M]}$ for $\text{H}_3\text{P}-\text{Ni}(\text{CO})_3$:

$$\Delta q_i^{\text{frag}} = - \int \left(\frac{\Delta\rho_i}{\rho_{\text{frag}} + \rho_{\text{sumfrag}}} \right) d\tau \quad (4)$$

Positive/negative Δq_i^{frag} values indicate net charge transfer from/to the fragment in question. As the electronic redistributions $\Delta\rho_i$ sum to the deformation density $\Delta\rho$ (eq 2), by definition the fragment's formal charge Q^{frag} (being 0 for L and [M] here) plus all charge flow contributions Δq_i^{frag} equals its Hirshfeld fragment charge within the total molecule, $q_{\text{H}}^{\text{frag}}$:

$$Q^{\text{frag}} + \sum \Delta q_i^{\text{frag}} = q_{\text{H}}^{\text{frag}} \quad (5)$$

In this work, we chose to calculate $\Delta q_i^{[M]}$ with respect to the transition-metal fragment [M], as it remains very similar across all studied ligands, thus keeping any numerical errors more systematic; these values were then negated to get the Δq_i^{L} with respect to the ligand (hereafter simply denoted Δq_i).

In the course of our research, the group of Tarantelli published the closely related charge-displacement analysis,^{5b,22} in which the NOCV electronic redistributions $\Delta\rho_i$ are partitioned simply by a plane that is moved (typically) along

the bonding axis. The resulting charge-displacement functions provide a detailed description of the bonding character, and their applicability appears promising. Then again, we think that our approach offers the following merits. First and foremost, proper partitioning is warranted also when one or both fragments bear groups that protrude toward the other fragment, as is the case for e.g. ortho-substituted NHC complexes. Conversely, the charge-displacement functions are contaminated by contributions from intrafragment polarizations on such substituents at positions where the partitioning plane happens to cut through them. Second, the method presented here consolidates the spatially dependent charge displacements into a single number per bonding type, which are more amenable for use as quantifiers in comparative analyses as illustrated below, and their interpretation is more accessible to chemists outside this subfield.

Ligand Donor/Acceptor Ability. For all four classes of complexes, Figure 3 shows scatter plots of the L–[M] charge flows Δq_σ and $\sum \Delta q_\pi$, the latter being the sum of the two mutually orthogonal π contributions. The plots are quite similar (but see below), demonstrating the general applicability of the charge flow contributions Δq_i to describe ligand donor/acceptor abilities. Different ligand classes are readily distinguished, e.g. the isonitriles and CO (moderate σ donors but strong π acceptors), amines and pyridine (weak ligands in both respects), and the NHCs (strong σ donors but weak π acceptors). Further, the π -electron-poor pNHC²³ features large values for Δq_σ as well as for $-\sum \Delta q_\pi$ as expected for this strongly σ donating and π accepting ligand. Thus, the computed charge flows bear an intuitive, close connection to experimental chemists' parlance for organometallic complexes.

The series $\text{PH}_n\text{F}_{3-n}$, $\text{PH}_n\text{Me}_{3-n}$, and $\text{PMe}_n\text{Ph}_{3-n}$ ($n = 0-3$) have been connected by lines to highlight the substitution trends. Going from PH_3 to PMe_3 , as expected the σ donation (as quantified by Δq_σ) increases monotonically with the number of methyl groups, while the π backbonding ($-\sum \Delta q_\pi$) decreases only slightly. However, replacement of methyls by phenyl groups (from PMe_3 to PPh_3) hardly affects the charge flow contributions. This suggests that, at least in their complexes with metal carbonyls, alkyl- and arylphosphines have similar σ -donor and π -acceptor properties—that is, their differing coordinating strengths must in large part be due to steric effects.^{2b} This is supported by the similar TEPs of $\text{PMe}_n\text{Ph}_{3-n}$ as well as by their ETS bonding energy decompositions (see section 2.4 in the Supporting Information): e.g., the $\text{Me}_3\text{P}-\text{Ni}(\text{CO})_3$ total “steric” interactions E_0 are 2.8 kcal mol⁻¹ less weakening but the total orbital interactions E_{oi} are only 1.5 kcal mol⁻¹ stronger than for the PPh_3 analogue.

The fluorine substitution trend shows more interesting features, which we will first discuss for the Ni, Fe, and W complexes. Going from PH_3 to PF_3 , we find that the π backbonding ($-\sum \Delta q_\pi$) increases significantly up to PHF_2 , but then for PF_3 it remains essentially the same while the σ -donation decreases markedly. This strongly nonmonotonic behavior is not at all apparent from the TEPs of the fluorophosphines that follow a closely linear trend (calculated $\nu_{\text{CO}}(\text{A}_1)$ for $\text{H}_n\text{F}_{3-n}\text{P}-\text{Ni}(\text{CO})_3$: 2047.35, 2055.89, 2064.85, and 2073.71 cm⁻¹ for $n = 0-3$, respectively). This is because the TEP expresses only the net donor ability of a ligand: i.e., a reduction in σ donation has a similar effect on the $\nu_{\text{CO}}(\text{A}_1)$ as does an increase in π backbonding. Thus, the TEP is a poor predictor for coordinating properties and applications in which σ - versus π -induced effects are quite distinct from those in L–

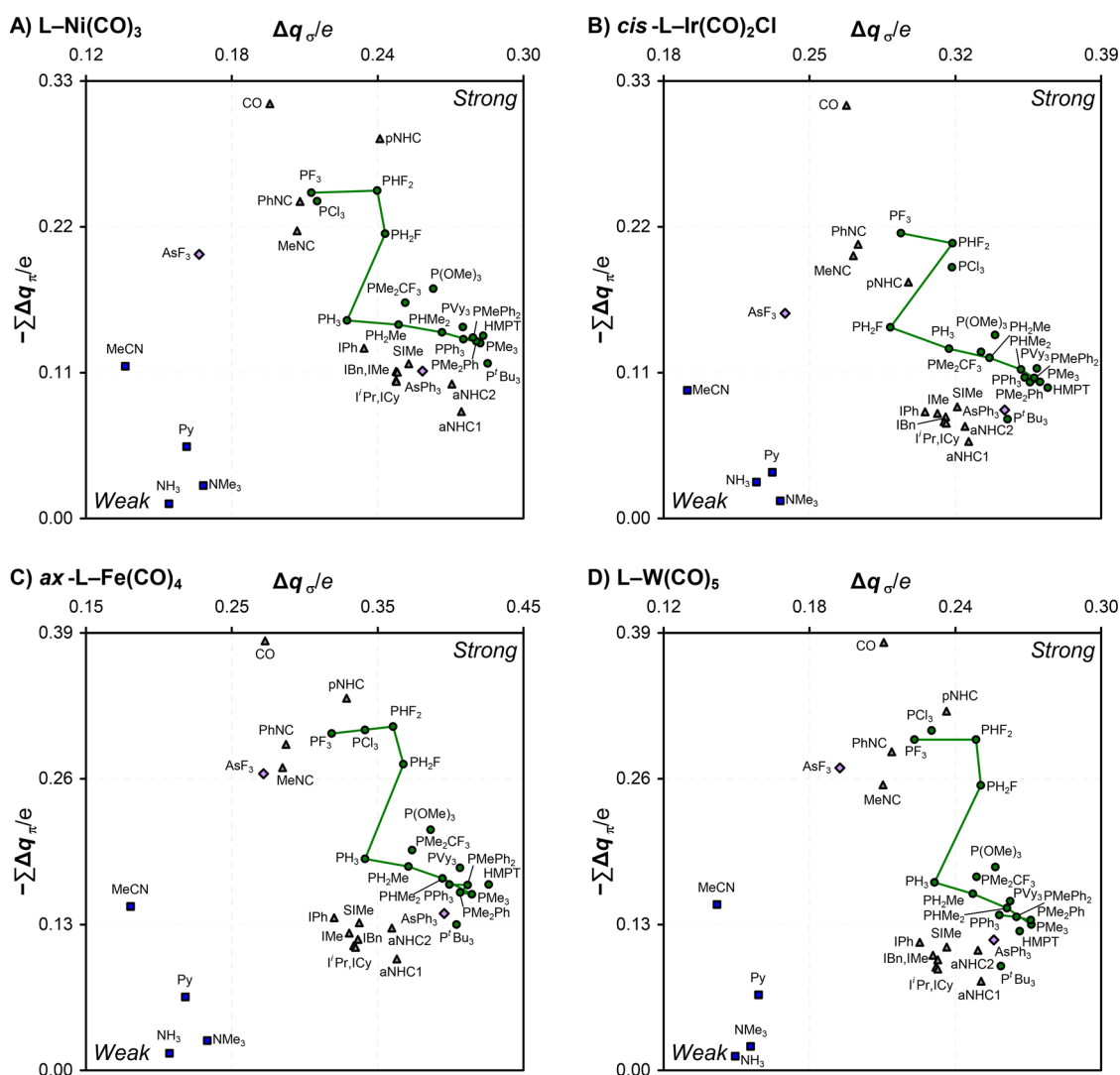


Figure 3. Scatter plots of σ -donor and π -acceptor charge flows in the $L-[M]$ bonding. Marker styles indicate the ligand's coordinating element (gray, C; blue, N; green, P; violet, As); lines connect the series PH_nF_{3-n} , PH_nMe_{3-n} , and PMe_nPh_{3-n} ($n = 0-3$).

$Ni(CO)_3$,^{1c,5b,22a,b} as may be the case with e.g. the reactivity of transition-metal catalysts.

In comparison to the other three classes of complexes, the substitution trend for $cis-(PH_nF_{3-n})Ir(CO)_2Cl$ ($n = 0-3$) shows a prominent exception. The $cis-H_2FP-Ir(CO)_2Cl$ bonding features much less σ donation and only slightly more π backbonding than that in $cis-H_3P-Ir(CO)_2Cl$. Inspection of the NOCV electronic redistributions reveals that this is due to donation from a lone electron pair on chlorine into the opposite $P-F \sigma^*$ antibond (Figure 4), as also reflected by the rather acute $P-Ir-Cl$ angle of 71.75° in $cis-(PH_2F)Ir(CO)_2Cl$ versus 81.35° in $cis-(PH_3)Ir(CO)_2Cl$.

To a lesser extent, similar $Cl: \rightarrow L \sigma^*$ interactions are found in the $cis-Ir(CO)_2Cl$ complexes of AsF_3 , PCl_3 , PHF_2 , PH_nMe_{3-n} ($n = 0-3$), and PMe_2CF_3 , whereas those of NH_3 , $pNHC$, and P^tBu_3 feature a $Cl \cdots H-N$ or $Cl \cdots H-C^{Me}$ ancillary contact. Indeed, for almost all of these ligands, differences are apparent between the scatter plots of charge flows for $L-Ni(CO)_3$ and $cis-L-Ir(CO)_2Cl$ (cf. Figure 3A vs Figure 3B). These secondary interactions compromise the transferability of the charge flows from the nickel carbonyl complexes to $cis-(L)Ir(CO)_2Cl$, and more in general they signify the challenge of empirically

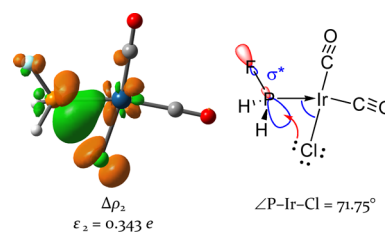


Figure 4. (left) Second-largest electronic redistribution for the $cis-H_2FP-Ir(CO)_2Cl$ bonding (± 0.002 au contours). (right) Schematic depiction of the $Cl: \rightarrow P-F \sigma^*$ interaction.

modeling ligand effects accurately using a knowledge base with a limited set of generic parameters.

Transferability of Δq_σ and Δq_π across Metal Complexes. To assess the transferability of the charge flow contributions, we performed linear regressions among all four series of complexes under study, as shown in Figure 5. The intercepts are all rather small and statistically significant only in some cases, but for consistency we chose to perform all regressions with intercept. The Δq_σ values for the Ir, Fe, and W complexes correlate well with those for $L-Ni(CO)_3$, certainly considering the wide scope of ligands investigated here. In

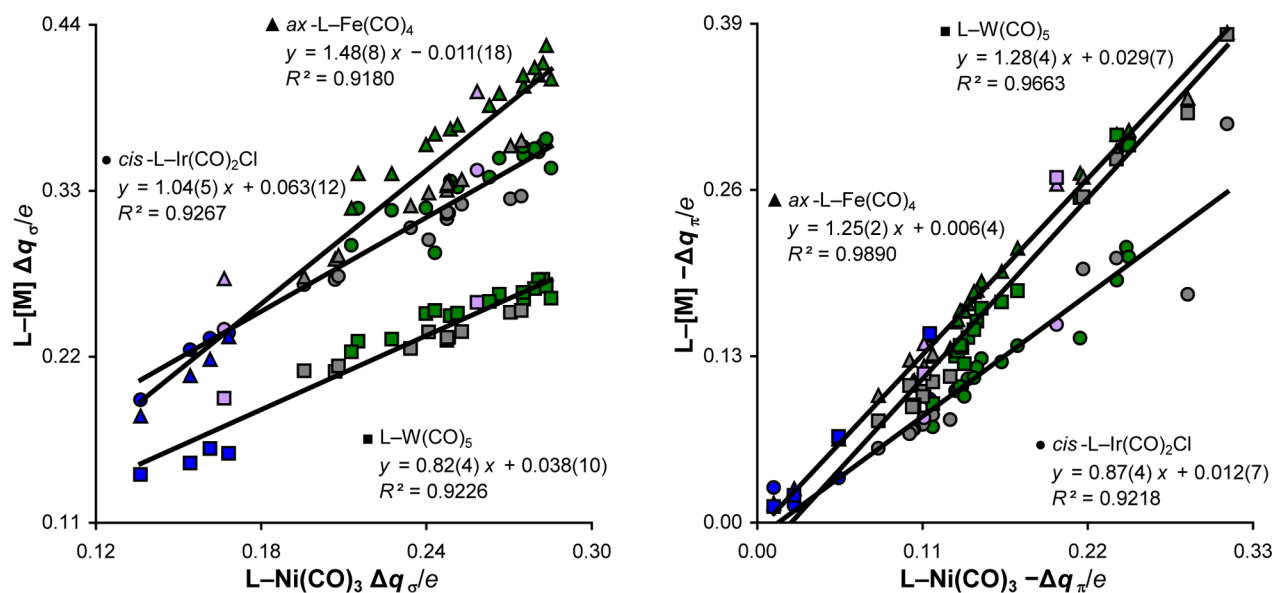


Figure 5. Linear regressions for the σ -donor (left) and π -acceptor (right) charge flows in the $L-[M]$ bonding. Marker colors indicate the ligand's coordinating element (gray, C; blue, N; green, P; violet, As).

addition, the $-\sum\Delta q_{\pi}$ values for the Fe and W complexes correlate particularly well with those for $L-Ni(CO)_3$, while those for $cis-L-Ir(CO)_2Cl$ show somewhat more scatter due to the mixed-in secondary interactions discussed above. As long as one stays alert for such specific interactions with ancillary ligands, the charge flows Δq_{σ} and $-\sum\Delta q_{\pi}$ appear to be well transferable to other complexes, having different coordination geometries. This renders them promising candidates for ligand knowledge bases as quantitative descriptors of the σ -donor and π -acceptor abilities.

Analogous to Hammett correlations for aryl derivatives that afford relative reaction constants from the slopes of the substituent trends,²⁴ the linear regressions in Figure 5 reveal how the charge flows depend on the electronic properties of the transition-metal moieties. The slopes signify that the σ -accepting ability of $[M]$ increases in the order $W(CO)_5 < Ni(CO)_3 \approx Ir(CO)_2Cl < Fe(CO)_4$ and the π -donating ability in the order $Ir(CO)_2Cl < Ni(CO)_3 < Fe(CO)_4 \approx W(CO)_5$. One may envision that the regression coefficients relate to the charge on the transition-metal moiety, on the diffuseness, polarizability, and energy levels of the metal's valence orbitals, and on the ease by which electron density is transferred to or from the ancillary ligands. However, a more detailed investigation of these aspects is beyond the scope of the current study.

Correlation of Δq_{σ} and Δq_{π} with the TEP. We believe that the charge flow contributions may earn a broad scope of applicability as quantifiers of σ donation and π backbonding. As a prototypical example, we use them here to construct a model describing the TEP. At the same time, this affords a better understanding as to what constitutes the TEP.

We first compare our calculated ν_{CO} values with available experimental values (see Figure 6, the Experimental Section and section 3.1 in the Supporting Information). At the BP86/TZP level of theory a very good congruity is obtained, in agreement with previous findings using other DFT levels of theory.^{5a,6d,14k} Oftentimes a frequency scaling factor is applied to the calculated ν_{CO} , which in this case is near unity irrespective of whether experimental data for polar media (in

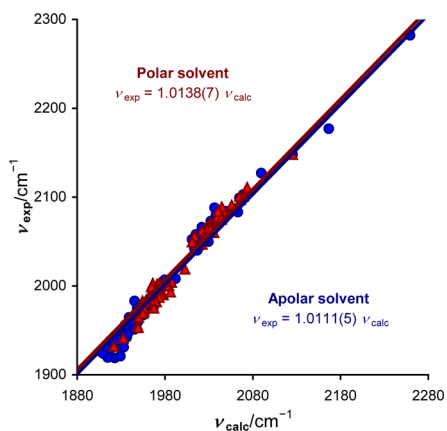


Figure 6. Regression analysis of experimental versus calculated carbonyl stretching frequencies. The good correlations justify the use of the BP86/TZP frequencies so as to include complexes that lack experimental data (see the main text).

most cases DCM) or apolar media (in most cases hexane) is used for the regression. This is in line with reports that postulate a fortuitous cancellation of model errors for BP86 frequencies.²⁰ The found strong congruity supports the use of the calculated ν_{CO} as indicators of the ligand electronic properties, allowing us to include complexes that have not yet been synthesized or for which the experimental data may be unreliable (see the remarks in section 3.1 of the Supporting Information). On the other hand, the complexes bearing (iso)nitriles as well as $Ni(CO)_4$ had to be left out because their TEP values are strongly affected by vibrational coupling with the ligand's $C\equiv X$ stretching mode.

While constructing a suitable multivariate regression model, we found that there is a dependence on the ligand's coordinating element. This dependence may have its origin in the Hirshfeld partitioning, which is performed using the densities of the isolated ligand and transition metal moieties. The resulting bias toward the neutral fragments²⁵ may not affect the partitioned properties equally in all cases—especially regarding the nature of the coordinating atoms, in whose

vicinity the largest changes in charge density occur. Thus, we decided to scale the ligand's charge flows Δq_σ and $-\sum \Delta q_\pi$ by the empirical factor f_{el} ($el = C, N, P, As$), where f_P is taken to be 1, as the TEP is based on the P-donor–Ni(CO)₃ complexes. The other scaling factors were optimized such as to minimize the sum of squared residuals of the multivariate model.

Furthermore, the inclusion of a steric parameter improves the model particularly for P^tBu₃ and the NHCs; the ortho substituents of the latter are approaching the metal carbonyl moiety and hence have a stronger steric interaction in comparison to most substituted phosphines. We chose to use %*V*_{bur}(Ni), the percentage of volume occupied by the ligand within a sphere of radius 3.50 Å around nickel in the BP86/ZORA/TZP computed structures of complexes L–Ni(CO)₃ (see also ref 19). Thus, the following multivariate regression model was obtained to fit the calculated $\nu_{CO}(A_1)$:

$$\begin{aligned} \nu_{\text{model}} (\text{cm}^{-1}) = & 2134(5) - 0.87(18) \times \%V_{\text{bur}}(\text{Ni}) \\ & - f_{el} \times [355(20) \times \Delta q_\sigma - 116(12) \\ & \times - \sum \Delta q_\pi] \end{aligned} \quad (6)$$

where $f_C = 1.278$, $f_N = 1.574$, $f_P \equiv 1$, and $f_{As} = 0.986$. For the 30 complexes (L)Ni(CO)₃ under consideration, this model affords a good R^2 value of 0.9684 ($\sigma_\nu = 3.7 \text{ cm}^{-1}$, Figure 7); F

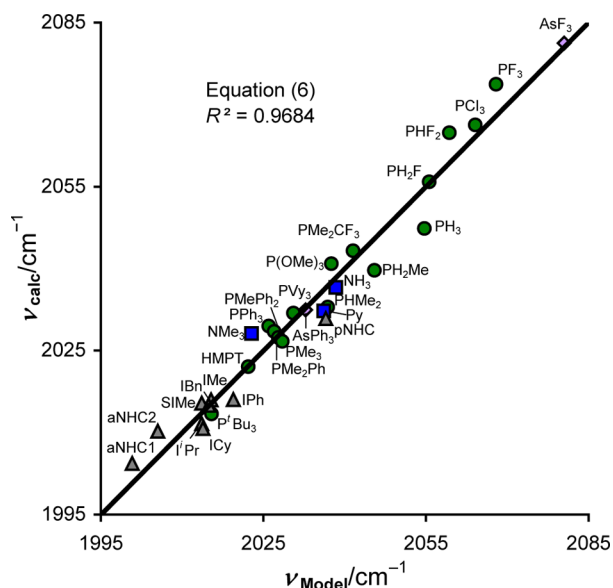


Figure 7. Application of charge flows to model the TEP according to eq 6. Marker colors indicate the ligand's coordinating element (gray, C; blue, N; green, P; violet, As).

tests with reduced models confirmed that all variables are significant (see section 3.4 of the Supporting Information). The scaling factors f_{el} appear to parallel the Pauling electronegativities χ_{el} of the coordinating elements; using $f_{el}' = (\chi_{el}/\chi_P)^{3/2}$ instead, the R^2 values decreases marginally to 0.9660 ($\sigma_\nu = 3.8 \text{ cm}^{-1}$). Further investigation is warranted as to whether this interesting finding has a more fundamental basis and whether a similar scaling may apply to other properties obtained through Hirshfeld partitioning. Equation 6 also indicates that the TEP is affected about 3 times more by an increase/decrease in σ donation than by an equivalent decrease/increase in π backbonding, as quantified by the charge flows Δq_σ and $-\sum \Delta q_\pi$ respectively.

We wish to stress that, again, the found congruity is exceptional considering the broad range of ligands included. Kégl et al.^{14k} recently published a systematic investigation on 12 P-donor Ni(CO)₃ complexes, correlating various computational parameters obtained from QTAIM, NBO, and ETS–NOCV analyses to the TEP. Most parameters performed clearly worse: only for the QTAIM delocalization index and the ETS–NOCV ΔE_σ did they find comparable R^2 values of 0.946 and 0.931, respectively—but note that, for our somewhat more diverse subset of 16 P-donor complexes, ΔE_σ performs not that well. If we model the calculated $\nu_{CO}(A_1)$ of just these 16 complexes using the charge flows Δq_σ and $-\sum \Delta q_\pi$ we do again obtain an excellent correlation ($R^2 = 0.9770$) even without a steric parameter.

Estimation of Δq_σ and Δq_π from Experimental Observables. We also sought expressions for the charge flows Δq_σ and $-\sum \Delta q_\pi$ in terms of CO stretching frequencies. Such relationships would allow estimating the σ -donor and π -acceptor abilities of yet other ligands from experimental observables. However, the phosphine vs NHC complexes in our data sets exhibit clearly different trends that could not be readily merged by including any commonly known ligand descriptor or by applying the aforementioned electronegativity-related scaling factors. The NHC complexes feature through-space interactions between the ligand's ortho substituents and nearby CO groups. Unsurprisingly, even the inclusion of a (nondirectional) steric parameter such as %*V*_{bur} into the model cannot properly account for such specific effects on the ν_{CO} values (see section 2.7 of the Supporting Information). For the current regression modeling we therefore decided to limit ourselves to the P-donor ligand series, for which the W(CO)₅ complexes afforded the smallest deviations. The regression variables were checked for significance, leading to the following optimal models (including a frequency scaling factor of 1.0125, taken as the average of the slopes in Figure 6):

$$\begin{aligned} \Delta q_{\sigma, \text{model}}(e) = & 6.8(5) + [3.8(5) \times \nu_{CO}(A_1) \\ & - 8.6(9) \times \nu_{CO}(A_1')] \\ & + 1.8(4) \times \nu_{CO}(B_1)] \times 10^{-3} \end{aligned} \quad (7)$$

$$\begin{aligned} -\sum \Delta q_{\pi, \text{model}}(e) = & [1.7(5) \times \%V_{\text{bur}} + 5.4(7) \times \nu_{CO}(E) \\ & + 6.6(8) \times \nu_{CO}(A_1) - 13.6(5) \times \nu_{CO}(A_1')] \\ & + 2.4(8) \times \nu_{CO}(B_1)] \times 10^{-3} \end{aligned} \quad (8)$$

For the 16 complexes under consideration, the model for Δq_σ afforded a good R^2 value of 0.9561 ($\sigma_\sigma = 3.4 \times 10^{-3} e$) and that for $-\sum \Delta q_\pi$ an even better R^2 value of 0.9921 ($\sigma_\pi = 7.0 \times 10^{-3} e$). Equations 7 and 8 both involve the frequency of the (approximately) B₁-symmetric CO stretching mode, which however is a forbidden transition in infrared absorption spectroscopy. On the other hand, all four relevant stretching modes of complexes (L)W(CO)₅ are Raman active (but one should bear in mind that these complexes are prone to photodecomposition). For the steric contribution in eq 8, %*V*_{bur} could be determined on the basis of the crystal structure of the ligand or of any complex thereof; several W(CO)₅ complexes are stable, crystallizable solids. Thus, the models described above provide a tool to experimentalists to disentangle the σ -donor and π -acceptor contributions in the dative bonding of P-donor ligands using physical observables. Notably, already before Tolman published his seminal work on

the $\text{Ni}(\text{CO})_3$ complexes,² Cotton and Kraihanzel related the spectroscopic properties of some $(\text{L})_n\text{W}(\text{CO})_{6-n}$ complexes to the ligand's electronics.²⁶

Note on Separability of Charge Flow Contributions.

As illustrated above, the ETS–NOCV–charge flow analysis may become a straightforward yet powerful diagnostic tool for computational chemists. However, as with all computational analyses, one should be cautious to use it as a black box. Namely, the NOCV decomposition may yield linear combinations of bonding interactions with (nearly) degenerate electronic redistributions $\Delta\rho_i$, in which case the derived charge flow contributions Δq_i are of course also admixtures. This is unproblematic as long as the bonding interactions in question are equivalent—for example, for the two π -backbonding contributions in the C_{3v} -symmetric $\text{H}_3\text{P}-\text{Ni}(\text{CO})_3$ (Figure 1, middle) any linear combination will afford the same, valid results. Illustrative, however, is the case of $\text{pNHC}-\text{Fe}(\text{CO})_4$, in which the electronic redistributions due to σ donation from the NHC's lone pair and to π backbonding into the NHC's π system happen to be nearly degenerate. This is indicated by closely similar NOCV eigenvalues ε (see Figure 8).

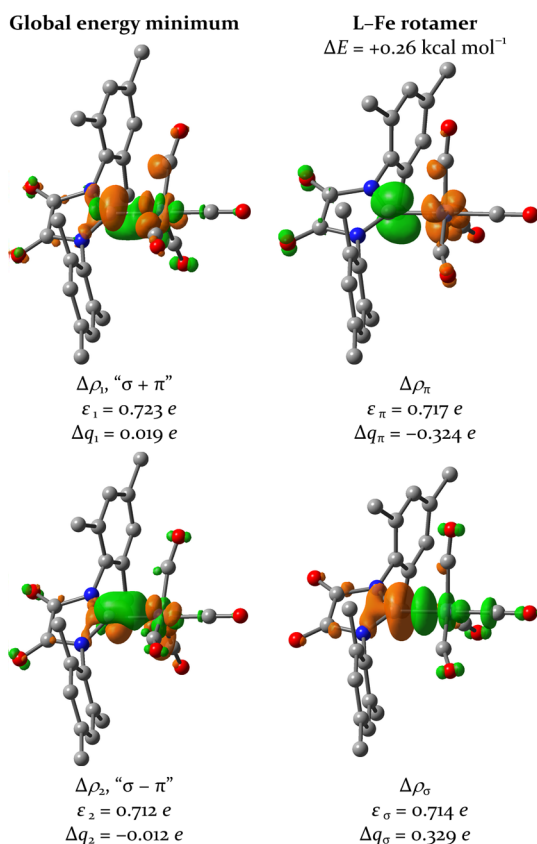


Figure 8. Primary electronic redistributions for the *ax*-pNHC– $\text{Fe}(\text{CO})_4$ bonding (± 0.004 au contours) in the two lowest-energy structures.

For the global energy minimum of *ax*-pNHC– $\text{Fe}(\text{CO})_4$ the NOCV decomposition affords approximately 1:1 linear combinations of the two bonding contributions, as shown in Figure 8 on the left.²⁷ As the admixed bonding modes have opposing dative character, the resulting charge flows are erroneously close to zero ($\Delta q_1 = 0.019 e$, $\Delta q_2 = -0.012 e$). The local minimum-energy structure shown in Figure 8 on the

right has the transition-metal moiety rotated by 30° and features a mirror plane through the NHC heterocycle, which facilitates the NOCV decomposition²⁸ into the desired σ and π contributions, as is directly apparent from the depicted electronic redistributions. The resulting charge flows are significantly nonzero at $\Delta q_\sigma = 0.392 e$ and $\Delta q_\pi = -0.324 e$, as expected for this strongly π accepting NHC ligand. These values should still be representative as electronic descriptors for pNHC in its axial coordination to $\text{Fe}(\text{CO})_4$, as the L–Fe rotamer is a mere $0.26 \text{ kcal mol}^{-1}$ higher in energy than the global energy minimum (at BP86/ZORA/TZP), and in solution the complex will undergo rapid L–Fe rotation regardless.

In summary, the NOCV electronic redistributions $\Delta\rho_i$ should always be visually inspected (e.g., through ADFview^{17a} or using any CUBE file visualization software) to ensure their correct assignment to specific bonding modes. We note that this caveat applies not just to the charge flow analysis presented here but to all analyses based on NOCV decomposition (and, in general, to any matrix diagonalization with potentially degenerate solutions).

CONCLUSIONS

A comprehensive range of transition-metal carbonyl complexes $\text{L}-[\text{M}]$, comprising different ligand classes, transition metals, and coordination geometries, was studied by DFT calculations. ETS–NOCV analysis describes the ligand–metal bonding interaction in such complexes by a set of characteristic electronic redistributions, which are readily assigned as e.g. σ -donating and π -backbonding interactions by visual inspection and which extend over the whole complex. The charge flow contributions Δq_σ and Δq_π introduced in this article follow intuitively from Hirshfeld partitioning of these electronic redistributions between the ligand and the metal fragment. With its implementation in ADF2017, the charge flow analysis can now straightforwardly be applied in extension to the ETS–NOCV bonding decomposition scheme.

While they are rooted in rigorous theoretical procedures, Δq_σ and Δq_π reflect the parlance of inorganic and organometallic chemists to describe ligand–metal bonding in terms of the extents of σ -electron donation and π -electron backbonding. The charge flow contributions reconfirm common perceptions regarding ligand electronic properties and are well transferable across the studied complexes, comprising a wide variety of ligands. As such, they appear promising for ligand knowledge bases as quantifiers of the ligand's σ -donor and π -acceptor abilities, going beyond the TEP, which only reflects the *net* donor strength of a ligand. In terms of Δq_σ and Δq_π (Table S6 in the Supporting Information) the TEP is affected 3 times more strongly by σ donation than by π backbonding—but applications e.g. in homogeneous catalysis may require a different ratio.

TEP values have recently been derived for several NHCs from the CO stretching frequencies of their *cis*- $\text{Ir}(\text{CO})_2\text{Cl}$ complexes or the rhodium analogues,⁴ but our analyses of such species revealed direct $\text{Cl} \rightarrow \text{L} \sigma^*$ interactions for various ligands, which compromises the transferability of their descriptors to other types of complexes. Apart from that, the good correlations of Δq_σ and Δq_π across different transition-metal series suggest that σ -acceptor and π -donor scales can also be created for the metal fragments. Moreover, the derived empirical relationships to the CO stretching frequencies of complexes $(\text{L})\text{W}(\text{CO})_5$ and $\%V_{\text{bur}}$ allow estimation of the σ -

donor and π -acceptor abilities of phosphines on the basis of experimental data. This further supports the use of the charge flow contributions in the design of novel ligands and complexes.

■ ASSOCIATED CONTENT

📄 Supporting Information

The Supporting Information is available free of charge on the ACS Publications website at DOI: 10.1021/acs.organomet.7b00365.

Experimental and computational details, optimized energies, frequencies, bonding energy decompositions and charge flows, contours of selected electronic redistributions, and regression analyses (PDF)

Cartesian coordinates of the calculated structures (XYZ)

■ AUTHOR INFORMATION

Corresponding Author

*P.C.: tel, +41-44-632-2898; e-mail, peter.chen@org.chem.ethz.ch.

ORCID

Yu-Ying Lai: 0000-0002-1921-6923

Peter Chen: 0000-0002-9280-4369

Present Addresses

[‡]Thermo Fisher (Bremen) Scientific, Hanna-Kunath-Straße 11, D-28199 Bremen, Germany.

[§]Institute of Polymer Science and Engineering, National Taiwan University, No. 1, Sec. 4, Roosevelt Road, Taipei, 10617 Taiwan.

Author Contributions

[†]E.P.A.C. and Y.-Y.L. contributed equally.

Notes

The authors declare no competing financial interest.

■ ACKNOWLEDGMENTS

We acknowledge support of this work by the ETH Zürich and the Swiss National Science Foundation. We are grateful to SCM for implementing our method of Hirshfeld partitioning of the NOCV electronic redistributions into ADF, and we thank M. Mitoraj for fruitful discussions.

■ REFERENCES

- (1) Review articles: (a) Dröge, T.; Glorius, F. *Angew. Chem., Int. Ed.* **2010**, *49*, 6940–6952. (b) Fey, N.; Orpen, A. G.; Harvey, J. N. *Coord. Chem. Rev.* **2009**, *253*, 704–722. (c) Kühn, O. *Coord. Chem. Rev.* **2005**, *249*, 693–704.
- (2) (a) Tolman, C. A. *J. Am. Chem. Soc.* **1970**, *92*, 2953–2956. (b) Tolman, C. A. *J. Am. Chem. Soc.* **1970**, *92*, 2956–2965. (c) Tolman, C. A. *Chem. Rev.* **1977**, *77*, 313–348.
- (3) Selected references: (a) Mathew, P.; Neels, A.; Albrecht, M. *J. Am. Chem. Soc.* **2008**, *130*, 13534–13535. (b) Starosta, R.; Bažanová, B.; Barszczewski, W. *Dalton Trans.* **2010**, *39*, 7547–7555. (c) Tennyson, A. G.; Ono, R. J.; Hudnall, T. W.; Khramov, D. M.; Er, J. A. V.; Kamplain, J. W.; Lynch, V. M.; Sessler, J. L.; Bielawski, C. W. *Chem. - Eur. J.* **2010**, *16*, 304–315. (d) Hudnall, T. W.; Bielawski, C. W. *J. Am. Chem. Soc.* **2009**, *131*, 16039–16041. (e) Rosen, E. L.; Varnado, C. D., Jr.; Tennyson, A. G.; Khramov, D. M.; Kamplain, J. W.; Sung, D. H.; Cresswell, P. T.; Lynch, V. M.; Bielawski, C. W. *Organometallics* **2009**, *28*, 6695–6706. (f) Collins, M. S.; Rosen, E. L.; Lynch, V. M.; Bielawski, C. W. *Organometallics* **2010**, *29*, 3047–3053. (g) Hudnall, T. W.; Tennyson, A. G.; Bielawski, C. W. *Organometallics* **2010**, *29*, 4569–4578. (h) Moerdyk, J. P.; Bielawski, C. W. *Organometallics* **2011**, *30*, 2278–2284. (i) Chianese, A. R.;

Kovacevic, A.; Zeglis, B. M.; Faller, J. W.; Crabtree, R. H. *Organometallics* **2004**, *23*, 2461–2468. (j) Tonner, R.; Frenking, G. *Organometallics* **2009**, *28*, 3901–3905. (k) Gudat, D.; Hüp, S.; Szarvas, L.; Nieger, M. *Chem. Commun.* **2000**, 1637–1638. (l) Gusev, D. G. *Organometallics* **2009**, *28*, 6458–6461. (m) Urbina-Blanco, C. A.; Bantreil, X.; Clavier, H.; Slawin, A. M. Z.; Nolan, S. P. *Beilstein J. Org. Chem.* **2010**, *6*, 1120–1126. (n) Diebolt, O.; Fortman, G. C.; Clavier, H.; Slawin, A. M. Z.; Escudero-Adán, E. C.; Benet-Buchholz, J.; Nolan, S. P. *Organometallics* **2011**, *30*, 1668–1676. (o) Otto, S.; Roodt, A. *Inorg. Chim. Acta* **2004**, *357*, 1–10. (p) Baber, R. A.; Collard, S.; Hooper, M.; Orpen, A. G.; Pringle, P. G.; Wilkinson, M. J.; Wingad, R. L. *Dalton Trans.* **2005**, 1491–1498. (q) Iwatsuki, S.; Kashiwamura, S.; Kashiwabara, K.; Suzuki, T.; Takagi, H. D. *Dalton Trans.* **2003**, 2280–2292.

(4) (a) Chianese, A. R.; Li, X.; Janzen, M. C.; Faller, J. W.; Crabtree, R. H. *Organometallics* **2003**, *22*, 1663–1667. (b) Kelly, R. A., III; Clavier, H.; Giudice, S.; Scott, N. M.; Stevens, E. D.; Bordner, J.; Samardjiev, I.; Hoff, C. D.; Cavallo, L.; Nolan, S. P. *Organometallics* **2008**, *27*, 202–210. (c) Wolf, S.; Plenio, H. J. *Organomet. Chem.* **2009**, *694*, 1487–1492. (d) Fürstner, A.; Alcarazo, M.; Krause, H.; Lehmann, C. W. *J. Am. Chem. Soc.* **2007**, *129*, 12676–12677.

(5) (a) Gusev, D. G. *Organometallics* **2009**, *28*, 763–770. (b) Ciancaleoni, G.; Scafuri, N.; Bistoni, G.; Macchioni, A.; Tarantelli, F.; Zuccaccia, D.; Belpassi, L. *Inorg. Chem.* **2014**, *53*, 9907–9916. (c) Valyaev, D. A.; Brousses, R.; Lugan, N.; Fernández, I.; Sierra, M. A. *Chem. - Eur. J.* **2011**, *17*, 6602–6605. (d) Kalescky, R.; Kraka, E.; Cremer, D. *Inorg. Chem.* **2014**, *53*, 478–495. (e) Setiawan, D.; Kalescky, R.; Kraka, E.; Cremer, D. *Inorg. Chem.* **2016**, *55*, 2332–2344.

(6) (a) Bartholomew, J.; Fernandez, A. L.; Lorsbach, B. A.; Wilson, M. R.; Prock, A.; Giering, W. P. *Organometallics* **1996**, *15*, 295–301. (b) Fernandez, A. L.; Wilson, M. P.; Prock, A.; Giering, W. P. *Organometallics* **2001**, *20*, 3429–3435. (c) Wilson, M. R.; Prock, A.; Giering, W. P.; Fernandez, A. L.; Haar, C. M.; Nolan, S. P.; Foxman, B. M. *Organometallics* **2002**, *21*, 2758–2763. (d) Perrin, L.; Clot, E.; Eisenstein, O.; Loch, J.; Crabtree, R. H. *Inorg. Chem.* **2001**, *40*, 5806–5811. (e) Suresh, C. H.; Koga, N. *Inorg. Chem.* **2002**, *41*, 1573–1578. (f) Kühn, O.; Lifson, K.; Langel, W. *Eur. J. Org. Chem.* **2006**, *2006*, 2336–2343. (g) Mathew, J.; Suresh, C. H. *Inorg. Chem.* **2010**, *49*, 4665–4669. (h) Coll, D. S.; Vidal, A. B.; Rodrigues, J. A.; Ocampo-Mavárez, E.; Añez, R.; Sierraalta, A. *Inorg. Chim. Acta* **2015**, *436*, 163–168.

(7) Review articles: (a) Frenking, G.; Fröhlich, N. *Chem. Rev.* **2000**, *100*, 717–774. (b) Frenking, G.; Wichmann, K.; Fröhlich, N.; Loschen, C.; Lein, M.; Frunzke, J.; Rayón, V. M. *Coord. Chem. Rev.* **2003**, *238*–239, 55–82. (c) Macchi, P.; Sironi, A. *Coord. Chem. Rev.* **2003**, *238*–239, 383–412. (d) Cortés-Guzmán, F.; Bader, R. W. F. *Coord. Chem. Rev.* **2005**, *249*, 633–662. (e) Jacobsen, H.; Correa, A.; Poater, A.; Costabile, C.; Cavallo, L. *Coord. Chem. Rev.* **2009**, *253*, 687–703.

(8) (a) Bader, R. F. W. *Atoms in Molecules. A Quantum Theory*; Oxford University Press: Oxford, U.K., 1990. (b) Bader, R. F. W. *Chem. Rev.* **1991**, *91*, 893–928.

(9) (a) Reed, A. E.; Curtiss, L. A.; Weinhold, F. *Chem. Rev.* **1988**, *88*, 899–926. (b) Weinhold, F.; Landis, C. R. *Valence and Bonding: A Natural Bond Orbital Donor–Acceptor Perspective*; Cambridge University Press: Cambridge, U.K., 2005.

(10) (a) Dapprich, S.; Frenking, G. *J. Phys. Chem.* **1995**, *99*, 9352–9362. (b) Ehlers, A. W.; Dapprich, S.; Vyboishchikov, S. F.; Frenking, G. *Organometallics* **1996**, *15*, 105–117.

(11) (a) Bagus, P. S.; Hermann, K.; Bauschlicher, C. W. *J. Chem. Phys.* **1984**, *80*, 4378–4386. (b) Hermann, K.; Bagus, P. S.; Bauschlicher, C. W. *Phys. Rev. B: Condens. Matter Mater. Phys.* **1985**, *31*, 6371–6378.

(12) (a) Morokuma, K. *Acc. Chem. Res.* **1977**, *10*, 294–300. (b) Ziegler, T.; Rauk, A. *Inorg. Chem.* **1979**, *18*, 1755–1759. (c) Ziegler, T.; Rauk, A. *Inorg. Chem.* **1979**, *18*, 1558–1565. (d) Bickelhaupt, F. M.; Baerends, E. J. In *Reviews in Computational*

Chemistry; Lipkowitz, K. B., Boyd, D. B., Eds.; Wiley: New York, 2000; Vol. 15, pp 1–86.

(13) Selected references: (a) Mitoraj, M.; Michalak, A. *J. Mol. Model.* **2007**, *13*, 347–355. (b) Mitoraj, M.; Michalak, A. *Organometallics* **2007**, *26*, 6576–6580. (c) Michalak, A.; Mitoraj, M.; Ziegler, T. *J. Phys. Chem. A* **2008**, *112*, 1933–1939. (d) Mitoraj, M. P.; Michalak, A.; Ziegler, T. *J. Chem. Theory Comput.* **2009**, *5*, 962–975. (e) Mitoraj, M. P.; Michalak, A.; Ziegler, T. *Organometallics* **2009**, *28*, 3727–3733. (f) Srebro, M.; Mitoraj, M.; Michalak, A. *Can. J. Chem.* **2009**, *87*, 1039–1054. (g) Mitoraj, M. P.; Michalak, A. *Inorg. Chem.* **2010**, *49*, 578–582. (h) Mitoraj, M. P.; Parafiniuk, M.; Srebro, M.; Handzlik, M.; Buczek, A.; Michalak, A. *J. Mol. Model.* **2011**, *17*, 2337–2352. (i) Srebro, M.; Mitoraj, M. *Organometallics* **2009**, *28*, 3650–3655. (j) Mitoraj, M. P.; Zhu, H.; Michalak, A.; Ziegler, T. *Int. J. Quantum Chem.* **2009**, *109*, 3379–3386.

(14) Selected computational studies: (a) Frenking, G.; Pidun, U. *J. Chem. Soc., Dalton Trans.* **1997**, 1653–1662. (b) González-Blanco, Ö.; Branchadell, V. *Organometallics* **1997**, *16*, 5556–5562. (c) Diefenbach, A.; Bickelhaupt, F. M.; Frenking, G. *J. Am. Chem. Soc.* **2000**, *122*, 6449–6458. (d) Frenking, G. *J. Organomet. Chem.* **2001**, *635*, 9–23. (e) Frenking, G.; Wichmann, K.; Fröhlich, N.; Grobe, J.; Golla, W.; Le Van, D.; Krebs, B.; Läge, M. *Organometallics* **2002**, *21*, 2921–2930. (f) Adamo, C.; Lelj, F. *J. Chem. Phys.* **1995**, *103*, 10605–10613. (g) Jacobsen, H.; Correa, A.; Costabile, C.; Cavallo, L. *J. Organomet. Chem.* **2006**, *691*, 4350–4358. (h) Leyssens, T.; Peeters, D.; Orpen, A. G.; Harvey, J. N. *Organometallics* **2007**, *26*, 2637–2645. (i) Comas-Vives, A.; Harvey, J. N. *Eur. J. Inorg. Chem.* **2011**, *2011*, 5025–5035. (j) Cukrowski, L.; de Lange, J. H.; Mitoraj, M. *J. Phys. Chem. A* **2014**, *118*, 623–637. (k) Kégl, T. R.; Kollár, L.; Kégl, T. *Advances in Chemistry* **2016**, *2016*, No. 4109758.

(15) Hirshfeld, F. L. *Theor. Chem. Acc.* **1977**, *44*, 129–138.

(16) (a) Cotton, F. A.; Troup, J. M. *J. Am. Chem. Soc.* **1974**, *96*, 3438–3443. (b) Elzinga, J.; Hogeveen, H. *J. Chem. Soc., Chem. Commun.* **1977**, 705–706. (c) Schumann, H.; Opitz, J. *J. Organomet. Chem.* **1979**, *166*, 233–239.

(17) (a) *ADF2010.02*; SCM, Theoretical Chemistry, Vrije Universiteit: Amsterdam, The Netherlands; <http://www.scm.com>. (b) te Velde, G.; Bickelhaupt, F. M.; van Gisbergen, S. J. A.; Fonseca Guerra, C.; Baerends, E. J.; Snijders, J. G.; Ziegler, T. *J. Comput. Chem.* **2001**, *22*, 931–967. (c) Fonseca Guerra, C.; Snijders, J. G.; te Velde, G.; Baerends, E. J. *Theor. Chem. Acc.* **1998**, *99*, 391–403. (d) Berces, A.; Dickson, R. M.; Fan, L.; Jacobsen, H.; Swerhone, D.; Ziegler, T. *Comput. Phys. Commun.* **1997**, *100*, 247–262. (e) Jacobsen, H.; Berces, A.; Swerhone, D.; Ziegler, T. *Comput. Phys. Commun.* **1997**, *100*, 263–276. (f) Wolff, S. K. *Int. J. Quantum Chem.* **2005**, *104*, 645–659.

(18) Empirical post-SCF dispersion corrections were not applied, as accurate reproduction of experimental bonding energies is not the primary focus of this study. All computed properties discussed here are derived from the Kohn–Sham density only. In addition, the charge flow contributions (if appropriately decomposed) are not very sensitive to minor structural changes, as illustrated by the comparable results obtained for conformers.

(19) (a) Poater, A.; Cosenza, B.; Correa, A.; Giudice, S.; Ragone, F.; Scarano, V.; Cavallo, L. *Eur. J. Inorg. Chem.* **2009**, *2009*, 1759–1766. (b) Clavier, H.; Nolan, S. P. *Chem. Commun.* **2010**, *46*, 841–861.

(20) (a) Reiher, M. *Inorg. Chem.* **2002**, *41*, 6928–6935. (b) Neugebauer, J.; Hess, B. A. *J. Chem. Phys.* **2003**, *118*, 7215–7225.

(21) (a) Dewar, M. J. S. *Bull. Soc. Chim. Fr.* **1951**, *18*, C79. (b) Chatt, J.; Duncanson, L. A. *J. Chem. Soc.* **1953**, 2939–2947. See also refs 7a, 14d, and references therein.

(22) (a) Gaggioli, C. A.; Ciancaleoni, G.; Zuccaccia, D.; Bistoni, G.; Belpassi, L.; Tarantelli, F.; Belanzoni, P. *Organometallics* **2016**, *35*, 2275–2285. (b) Bistoni, G.; Belanzoni, P.; Belpassi, L.; Tarantelli, F. *J. Phys. Chem. A* **2016**, *120*, 5239–5247. (c) Bistoni, G.; Rampino, S.; Tarantelli, F.; Belpassi, L. *J. Chem. Phys.* **2015**, *142*, 084112. (d) Bistoni, G.; Belpassi, L.; Tarantelli, F. *Angew. Chem., Int. Ed.* **2013**, *52*, 11599–11602.

(23) Braun, M.; Frank, W.; Reiss, G. J.; Ganter, C. *Organometallics* **2010**, *29*, 4418–4420.

(24) (a) Hammett, L. P. *Chem. Rev.* **1935**, *17*, 125–136. (b) Hammett, L. P. *J. Am. Chem. Soc.* **1937**, *59*, 96–103. (c) Muller, P. *Pure Appl. Chem.* **1994**, *66*, 1119.

(25) (a) Bultinck, P.; van Alsenoy, C.; Ayers, P. W.; Carbó-Dorca, R. *J. Chem. Phys.* **2007**, *126*, 144111. (b) Verstraelen, T.; Ayers, P. W.; Van Speybroeck, V.; Waroquier, M. *J. Chem. Theory Comput.* **2013**, *9*, 2221–2225.

(26) (a) Cotton, F. A.; Kraihanzel, C. S. *J. Am. Chem. Soc.* **1962**, *84*, 4432–4438. (b) Kraihanzel, C. S.; Cotton, F. A. *Inorg. Chem.* **1963**, *2*, 533–540. (c) Jolly, W. L.; Avanzino, S. C.; Rietz, R. R. *Inorg. Chem.* **1977**, *16*, 964–966.

(27) Slight changes in the matrix diagonalization strategy for the NOCV analysis (e.g., the convergence criterion) or in the deformation density itself (e.g., calculation at a different level of theory) may affect the linear combinations of the near-degenerate σ - and π -type charge delocalizations.

(28) Note that the NOCV decomposition itself cannot use any symmetry operations.